

Out-of-plane heat transfer in van der Waals stacks through electron-hyperbolic phonon coupling

Klaas-Jan Tielrooij^{1*}, Niels C. H. Hesp¹, Alessandro Principi^{2,3}, Mark B. Lundeberg¹, Eva A. A. Pogna⁴, Luca Banszerus⁵, Zoltán Mics⁶, Mathieu Massicotte¹, Peter Schmidt¹, Diana Davydovskaya¹, David G. Purdie⁷, Ilya Goykhman⁷, Giancarlo Soavi⁷, Antonio Lombardo⁸, Kenji Watanabe⁸, Takashi Taniguchi⁸, Mischa Bonn⁶, Dmitry Turchinovich^{6,11}, Christoph Stampfer⁵, Andrea C. Ferrari⁷, Giulio Cerullo⁴, Marco Polini⁹ and Frank H. L. Koppens^{1,10*}

Van der Waals heterostructures have emerged as promising building blocks that offer access to new physics, novel device functionalities and superior electrical and optoelectronic properties¹⁻⁷. Applications such as thermal management, photodetection, light emission, data communication, high-speed electronics and light harvesting⁸⁻¹⁶ require a thorough understanding of (nanoscale) heat flow. Here, using time-resolved photocurrent measurements, we identify an efficient out-of-plane energy transfer channel, where charge carriers in graphene couple to hyperbolic phonon polaritons¹⁷⁻¹⁹ in the encapsulating layered material. This hyperbolic cooling is particularly efficient, giving picosecond cooling times for hexagonal BN, where the high-momentum hyperbolic phonon polaritons enable efficient near-field energy transfer. We study this heat transfer mechanism using distinct control knobs to vary carrier density and lattice temperature, and find excellent agreement with theory without any adjustable parameters. These insights may lead to the ability to control heat flow in van der Waals heterostructures.

Owing to its large in-plane thermal conductivity, graphene has been suggested as a material for the thermal management of nanoscale devices⁸. Graphene is also well known for its ability to convert incident light into electrical heat: hot electrons. These can be used to generate photocurrent, with applications in photodetection, data communication and light harvesting^{10,20,21}. Understanding and ultimately controlling heat flow in graphene–van der Waals heterostructures is of paramount importance. For example, the short cooling time of graphene hot carriers is advantageous for thermal management and for the high switching rates of photodetectors for data communication, whereas a long cooling time is favourable for photodetection sensitivity^{10,20,21}. Of particular relevance are heterostructure devices that contain high-quality graphene encapsulated by layered materials such as hexagonal BN (hBN) and MoS₂, which have the potential to improve the performance of electronic and optoelectronic devices^{1,2}.

A number of cooling pathways for graphene carriers have been proposed, involving, among others, strongly coupled optical phonons²²⁻²⁴, acoustic phonons²⁵⁻²⁸, substrate phonons²⁹ and plasmons³⁰ (Supplementary Section 1). Here, using several experimental approaches, we show that cooling in graphene encapsulated by hBN is governed by out-of-plane coupling of graphene electrons to special polar phonon modes that occur in layered materials (LMs)—hyperbolic phonon polaritons—where $\epsilon_{xx}\epsilon_{zz} < 0$ (ϵ_{xx} and ϵ_{zz} are the permittivities parallel and perpendicular to the LM plane). As a result of this property, these materials carry deep subwavelength, ray-like optical phonon polaritons. In hBN, a large number of hyperbolic phonon modes with high momenta exist within the two Reststrahlen bands, far outside the light cone. The most notable modes occur at energies of ~100 meV and ~180 meV (ref. 17), so energy overlap with the graphene hot-carrier distribution is substantial. The unusual hyperbolic character gives rise to a very high density of optical states and thus large thermal energy densities^{17,18}, thereby providing a potentially efficient cooling pathway for hot carriers in graphene. By near-field coupling between graphene and hBN, efficient energy transfer from hot carriers to hyperbolic phonon polaritons is possible³¹. Here, we show that the measured carrier dynamics of hBN-encapsulated graphene can be explained by this hyperbolic cooling process, as illustrated in Fig. 1a.

Ultrafast time-resolved photocurrent measurements were obtained from the hBN-encapsulated, Hall-bar-shaped, exfoliated graphene device shown in Fig. 1b. The device contains chemical-vapour-deposited (CVD) graphene split gates under the bottom hBN (thickness of 70 nm), generating a p–n junction in the middle of the device. A second hBN-encapsulated device with metallic split gates gave fully consistent results. With 800 nm light incident on the p–n junction, a photovoltage is generated by the photothermoelectric (PTE) effect^{20,21} (photocurrent and reflection data are shown in Supplementary Fig. 1 and the characteristic PTE sixfold pattern in Supplementary Fig. 2). By varying the delay Δt

¹ICFO – Institut de Ciències Fotòniques, The Barcelona Institute of Science and Technology, Castelldefels (Barcelona), Spain. ²Radboud University, Institute for Molecules and Materials, Nijmegen, The Netherlands. ³School of Physics & Astronomy, University of Manchester, Manchester, UK. ⁴IFN-CNR, Dipartimento di Fisica, Politecnico di Milano, Milano, Italy. ⁵JARA-FIT and 2nd Institute of Physics, RWTH Aachen University, Aachen, Germany. ⁶Max Planck Institute for Polymer Research, Mainz, Germany. ⁷Cambridge Graphene Centre, University of Cambridge, Cambridge, UK. ⁸National Institute for Material Science, Tsukuba, Japan. ⁹Istituto Italiano di Tecnologia, Graphene Labs, Genova, Italy. ¹⁰ICREA – Institució Catalana de Recerca i Estudis Avançats, Barcelona, Spain.

Present address: ¹¹Fakultät für Physik, Universität Duisburg-Essen, Duisburg, Germany. Klaas-Jan Tielrooij and Niels Hesp are equally contributing authors.

*e-mail: klaas-jan.tielrooij@icfo.eu; frank.koppens@icfo.eu

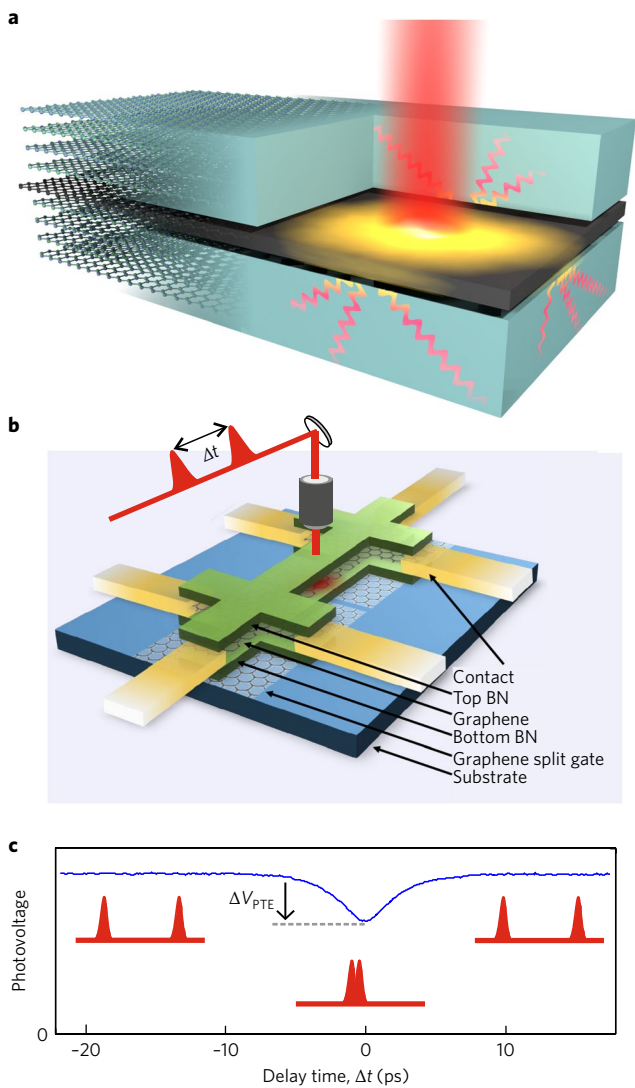


Fig. 1 | Hot carrier cooling in hBN-encapsulated graphene. **a**, Schematic representation of out-of-plane heat transfer in hBN-encapsulated graphene, with highly efficient near-field emission from graphene hot carriers into directional hyperbolic phonon polaritons of the encapsulating material. **b**, Schematic drawing of the hBN-encapsulated graphene device with graphene split gates. By applying different voltages to the two split gates we create a p–n junction in the encapsulated graphene layer, which we illuminate with two ultrafast pulses that arrive with variable time delay Δt . **c**, The resultant photo-thermoelectric photovoltage measured between the two contacts shows a dip when the two ultrafast pulses overlap. This is due to the nonlinear relation between hot carrier temperature and incident light intensity. The dynamics of the photovoltage dip ΔV_{PTE} as a function of time delay Δt therefore correspond to the cooling dynamics of the hot carriers at the p–n junction.

between two subpicosecond pulses we extracted the carrier dynamics from the photovoltage signal $\Delta V_{\text{PTE}}(\Delta t)$ (Fig. 1c). Because the PTE voltage scales with the light-induced increase in carrier temperature, the decay dynamics of $\Delta V_{\text{PTE}}(\Delta t)$ closely mimic the cooling dynamics of the hot electron system (see Supplementary Fig. 3 for an analysis of the extent to which the experimentally observed decay dynamics correspond to the underlying cooling dynamics). In the case of exponential decay dynamics, which we observe above a lattice temperature of ~ 200 K, we extracted

an experimental cooling timescale τ_{exp} by describing the decay dynamics with $\Delta V_{\text{PTE}}(\Delta t) \propto e^{-\Delta t/\tau_{\text{exp}}}$.

First, we electrically characterized our device using four-probe measurements (Fig. 2a) and found a mean free path of $k_{\text{F}}\ell = 80\text{--}100$ at a carrier density of $n = 1.7 \times 10^{12} \text{ cm}^{-2}$, corresponding to a mobility of $25,000\text{--}30,000 \text{ cm}^2 \text{ V}^{-1} \text{ s}^{-1}$ and momentum scattering time of $340\text{--}440$ fs. As expected, this is much higher than SiO_2 -supported devices with a typical $k_{\text{F}}\ell$ of <10 , mobility of $<5,000 \text{ cm}^2 \text{ V}^{-1} \text{ s}^{-1}$ and momentum scattering time of <100 fs (for example, ref. 27). In such devices, carrier cooling is typically ascribed to disorder-assisted cooling by scattering with graphene acoustic phonons^{26–28}.

To study hot-carrier cooling in our high-mobility, encapsulated devices we examined $\Delta V_{\text{PTE}}(\Delta t)$ while varying graphene's most characteristic parameter, carrier density n . In particular, we applied gate voltage $V_{\text{L}} = +V - V_{\text{D}}$ to the left split gate and $V_{\text{R}} = -V - V_{\text{D}}$ to the right gate, such that there was always either a p–n junction or an n–p junction, with equal electron and hole densities in the two graphene regions (V_{D} is the gate voltage corresponding to the Dirac point). The incident laser fluence was typically $5\text{--}40 \mu\text{J cm}^{-2}$. The data show that cooling becomes faster upon increasing the carrier density (Fig. 2b). We also varied the lattice temperature T_{L} and observed faster decay for increasing lattice temperature (Fig. 2c, taken at $n \approx 1 \times 10^{12} \text{ cm}^{-2}$). At low temperatures (below ~ 200 K), cooling is non-exponential, whereas at room temperature we observe exponential decay of the photovoltage dip, with a timescale of $\tau_{\text{exp}} \approx 2.5$ ps (for $n = 1.7 \times 10^{12} \text{ cm}^{-2}$). We independently verified this cooling time using two alternative measurement techniques that are both sensitive to electron-cooling dynamics, but in different ways (Supplementary Fig. 4). First, using ultrafast optical pump–optical probe spectroscopy, which probes interband transitions²⁴, we found $\tau_{\text{exp}} = 2.55$ ps for the decay of the absorption photobleaching. Second, using optical pump–terahertz probe spectroscopy, which probes intraband transitions¹³, we obtained $\tau_{\text{exp}} = 2.2$ ps for the decay of the photoconductivity. For these two experiments we used excitation conditions (incident pulse fluence of $8\text{--}20 \mu\text{J cm}^{-2}$) similar to those used in the photocurrent measurements, and the measurements were performed on two separate devices consisting of large-area, high-quality hBN-encapsulated CVD graphene, as in ref. 32. Thus, all three techniques consistently yield similar cooling times for hBN-encapsulated graphene.

We compared these observations with different cooling mechanisms and found that the data are qualitatively and quantitatively inconsistent with in-plane cooling by scattering with graphene acoustic phonons through normal²⁵ or disorder-assisted collisions^{26–28} (Supplementary Section 1 and Supplementary Fig. 5). In-plane cooling of high-energy carriers can also occur by scattering to graphene optical phonons, which typically occurs on a subpicosecond timescale^{22,24}. Reference 23 reports that for non-encapsulated graphene this channel gives picosecond decay dynamics for terahertz photoconductivity. However, these results deviate in several ways from our observations for hBN-encapsulated graphene (Supplementary Section 1). For example, we observed a twofold increase in cooling time by decreasing T_{L} from 300 K to 200 K, whereas optical phonon cooling gives cooling dynamics that are independent of substrate temperature (for $E_{\text{F}} = 0.3 \text{ eV}$), as shown in ref. 23. This indicates that, besides a fraction of hot graphene electrons possibly cooling through optical phonons, a different cooling mechanism plays an important role. Because we observe a striking effect of the hBN crystal slab thickness on the cooling dynamics (Supplementary Fig. 6 and Supplementary Section 2), we propose an out-of-plane cooling mechanism where hot graphene carriers lose their energy to remote polar phonons in the encapsulating layered material. The energy transfer can be understood from fluctuation electrodynamics, where any process that dissipates energy in the form of heat has a reverse process that is driven by thermal fluctuations and thus becomes stronger at higher temperatures^{33,34}. An example of such

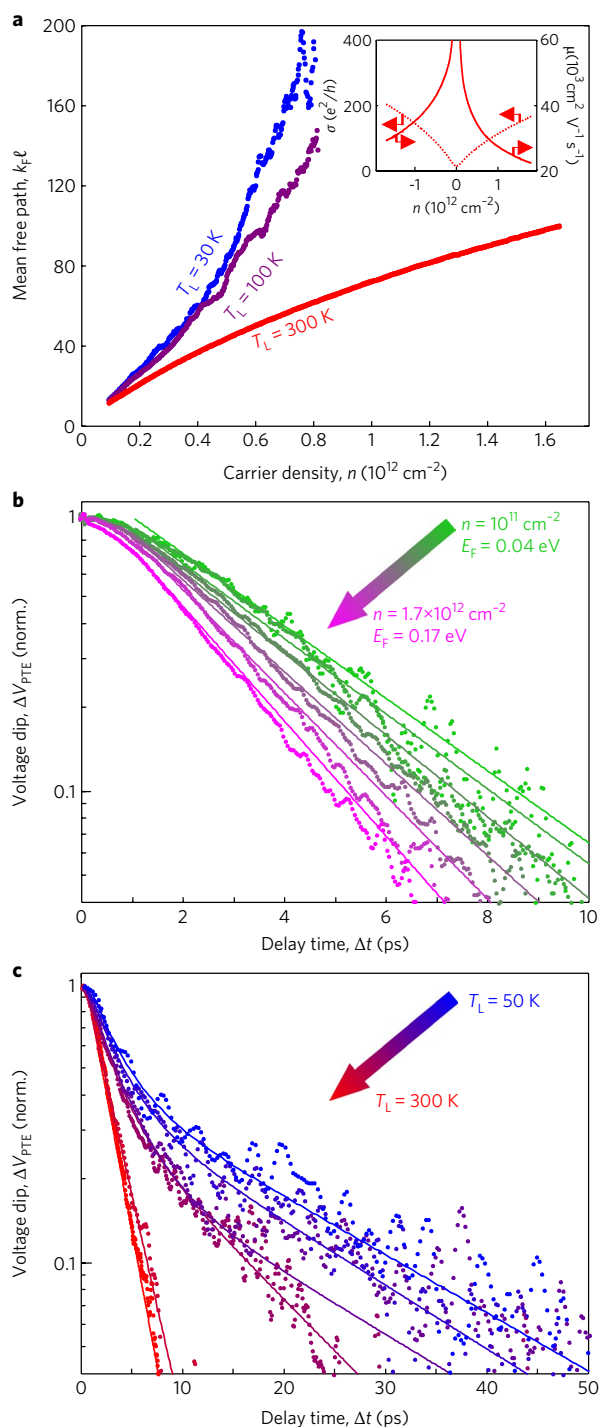


Fig. 2 | Effect of doping and lattice temperature. **a**, From four-probe transport measurements, we extract the dimensionless mean free path parameter $k_F l$ as a function of carrier density for three different lattice temperatures. These data show that carrier scattering in our hBN-encapsulated graphene is much less efficient than in SiO₂-supported graphene where $k_F l$ is typically 10 or less and where disorder-assisted supercollisions constitute the dominant cooling mechanism^{26–28}. Inset: Conductivity and mobility versus gate-induced carrier density. By comparing four-probe and two-probe measurements we find that each contact has a contact resistance of 5–8 kΩ. **b, c**, Dynamics of the photovoltage dip ΔV_{PTE} , showing that hot-carrier cooling becomes faster upon increasing the carrier density (**b**) and upon increasing the lattice temperature (**c**). In **b**, measurements are taken at a lattice temperature of $T_L = 300$ K and in **c** at a carrier density of $n \approx 1.7 \times 10^{12} \text{ cm}^{-2}$. Solid lines are bi-exponential guides to the eye.

paired processes is light absorption and blackbody radiation, which means that graphene emits thermal noise due to the dissipative real part (indicated by \mathcal{R}) of the frequency- and momentum-dependent optical sheet conductivity $\sigma(\omega, k)$. This thermal noise is efficiently absorbed by hBN, hBN being a lossy polarizable material, leading to an energy transfer rate of³¹

$$Q = \int \int \int_{-\infty}^{\infty} \frac{d\omega dk_x dk_y}{(2\pi)^3} [n_B(\omega, T_e) - n_B(\omega, T_L)] M(\omega, k), \quad (1)$$

where $n_B(\omega, T) = \frac{\hbar\omega}{e^{\hbar\omega/k_B T} - 1}$ and $M(\omega, k) = 4 \frac{\mathcal{R}\{Y(\omega, k)\} \mathcal{R}\{\sigma(\omega, k)\}}{|Y(\omega, k) + \sigma(\omega, k)|^2}$ (k_B is Boltzmann’s constant). Heat transfer from hot graphene electrons to hBN hyperbolic phonon polaritons is thus governed by the Bose factor $[n_B(\omega, T_e) - n_B(\omega, T_L)]$, which describes the energy disequilibrium between hot graphene carriers and the cold hBN phonon system and the impedance-matching function $M(\omega, k)$, which is non-zero when the surface admittance $Y(\omega, k)$ has a non-zero real part. We calculated $Y(\omega, k)$ as in ref.³⁵ (see Methods for details) and found that, near the hyperbolic hBN phonon frequencies, $Y(\omega, k)$ is real over a large k -space area and a relatively wide frequency band. Because $\sigma(\omega, k)$, calculated using the random phase approximation³⁶, also has a significant real part, this leads to an impedance-matching function M approaching unity. Due to this near-field coupling to hyperbolic modes, the heat conductivity exceeds Planck’s law for blackbody radiation by orders of magnitude (Supplementary Fig. 7). The reason for this is that, in vacuum, the k -space for blackbody radiation is limited to $k < \omega/c$ (where c is the speed of light in vacuum), whereas this restriction is lifted in the near-field interaction with hBN hyperbolic phonon polaritons. This super-Planckian coupling to hyperbolic hBN phonons thus provides a highly efficient cooling channel for hot carriers in graphene. Cooling to hyperbolic modes also occurs in materials such as MoS₂, although there it is not as efficient as for hBN (Supplementary Fig. 7).

To compare our hyperbolic cooling theory with the experimental data, we examined the calculated energy transfer rate Q . Here, solving equation (1) gives cooling dynamics with a cooling timescale

$$\tau_{\text{calc}}(T_e, T_L) = C_n \frac{T_e - T_L}{Q}, \quad (2)$$

where C_n is the electronic heat capacity of graphene at constant n (ref.³¹). In the limit of weak heating, where T_e approaches T_L , we obtain exponential decay with the near-equilibrium timescale $\tau_{\text{calc}}(T_e \rightarrow T_L) = \tau_{\text{calc}}^* = C_n \left(\frac{\partial Q}{\partial T_e} \Big|_{T_e = T_L} \right)^{-1}$, where $\frac{\partial Q}{\partial T_e} \Big|_{T_e = T_L}$ is the interfacial heat conductivity Γ . We compared the calculated near-equilibrium cooling time τ_{calc}^* with the measured exponential decay time τ_{exp} (Fig. 3), although strictly speaking these experimental timescales correspond to the strong heating regime, where $T_e \gg T_L$. The reason for this is that our technique is not sensitive enough at low incident powers, which means that we cannot experimentally directly access the near-equilibrium cooling time τ_{calc}^* . Nevertheless, we find that our hyperbolic hBN cooling model semi-quantitatively reproduces the experimentally observed trends for the entire range of investigated carrier densities (up to $1.6 \times 10^{12} \text{ cm}^{-2}$) and lattice temperatures (200–300 K). In particular, cooling slows down for lower lattice temperatures, which we attribute mainly to the smaller Bose factor in equation (1) and thus smaller energy transfer rate Q . The calculations also reproduce the observation of a longer cooling time around the Dirac point. This is the result of the energy transfer rate Q smoothly decreasing towards zero carrier density, while the electronic heat capacity C_n flattens around the Dirac point towards its neutral graphene value (Supplementary

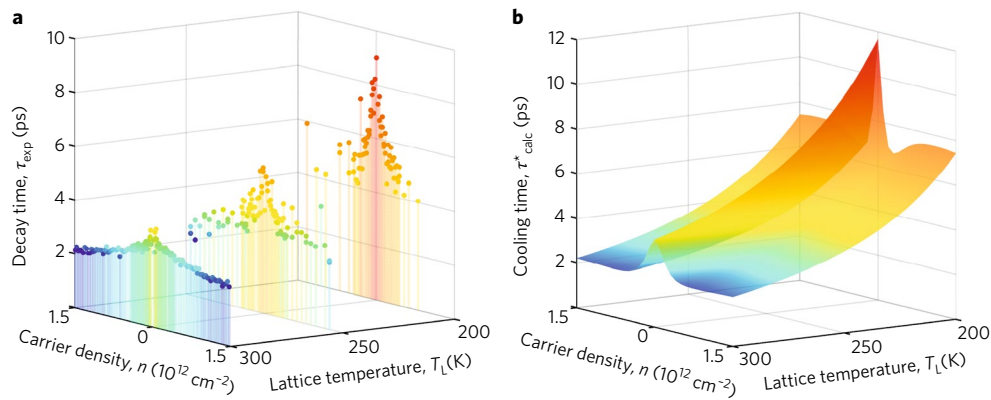


Fig. 3 | Qualitative comparison with hyperbolic hBN cooling. a, b, Comparison between experimental decay time τ_{exp} extracted from the dynamics of the photovoltage dip (**a**) and the predicted near-equilibrium cooling time τ_{calc}^* for super-Planckian cooling to hyperbolic hBN phonons (**b**). Both in experiment and theory we vary the carrier density and lattice temperature.

Fig. 7). At higher carrier densities ($n = 1 \times 10^{12} \text{ cm}^{-2}$) the increasing energy transfer rate is compensated by the increasing heat capacity, leading to a weak dependence of cooling time on carrier density. Cooling to hyperbolic modes was also observed in a noise thermometry study³⁷. We further note that the two distinct hyperbolic modes contribute almost equally to the overall cooling time, with the lower-energy mode slightly dominant (Supplementary Fig. 7). This can be attributed to more energy overlap in the Bose factor. We note that the hyperbolic cooling model reproduces the observed slower decay dynamics for encapsulation with very thin hBN flakes (Supplementary Fig. 6). In this case, cooling is slower because, overall, there is a lower density of hyperbolic modes to which to couple.

To make a more quantitative comparison, we took into account that the measurements are typically carried out in the strong heating regime, where $T_e \gg T_L$. We first measured the cooling dynamics for increasing laser power and estimated the electron temperatures that correspond to each power from the characteristic power-dependent photoresponse (Supplementary Fig. 8 and Methods), thus obtaining the exponential decay time τ_{exp} versus T_e (Fig. 4a). In the experimentally accessible regime ($\Delta T_e = T_e - T_L > 200 \text{ K}$), τ_{exp} increases with increasing T_e (measured for $n = 1.2 \times 10^{12} \text{ cm}^{-2}$). We compared this with the calculated cooling time τ_{calc} , which describes the ‘instantaneous’ cooling time at a certain T_e and found quantitative agreement without any adjustable parameters. The reason for the increasing cooling time with increasing T_e can be seen from equation (2) and by noting that $Q/(T_e - T_L)$ scales roughly linearly with $(T_e - T_L)$. At the same time, the electronic heat capacity C_n increases more than linearly with increasing T_e for large T_e . This leads to a net increase in the cooling time with increasing T_e . The agreement between experiment and calculation prompted us to make a more quantitative comparison for varying carrier density n . Figure 4b shows τ_{exp} for three different laser powers ($P = 21, 47$ and $94 \mu\text{W}$), corresponding to three different initial hot electron temperatures ($\Delta T_e = 650, 950$ and $1,250 \text{ K}$), together with the calculated near-equilibrium cooling time τ_{calc}^* . The comparison between experimental results in the strong heating regime (τ_{exp}) and theoretical results close to equilibrium (τ_{calc}^*) is justified in Fig. 4a, where we show that the cooling time at $T_e \approx 1,000 \text{ K}$ is similar to τ_{calc}^* . Again, we find agreement between experiment and theory without any adjustable parameters.

Finally, we compared the calculated time-domain cooling dynamics in the strong heating regime directly with the measured photocurrent dynamics. The calculated cooling dynamics describe cooling from an initial T_e down to T_L , as constructed from the

electron temperature-dependent cooling time τ_{calc} in equation (2). We compared these calculated cooling dynamics directly with the measured photovoltage dynamics $\Delta V_{\text{PTE}}(\Delta t)$ for six different lattice temperatures at a low carrier density of $n = 0.06 \times 10^{12} \text{ cm}^{-2}$ (Fig. 4c). Using the initial temperature (at the p–n junction) as a fit parameter, we found that the hyperbolic cooling model can describe the experimental data very well. At room temperature, the initial temperature is similar to the one we calculated (Supplementary Fig. 8), whereas we find a lower initial temperature at lower lattice temperatures. This is due to the increased mechanical vibrations of the sample and lateral heat diffusion out of the laser spot at lower T_L , which both lead to a larger photocurrent spot size and thus a lower effective initial T_e at the p–n junction (Supplementary Fig. 9). For a lattice temperature of 50 K , we furthermore see an increasing discrepancy for a delay time 15 ps , which most probably indicates that hBN phonons alone do not account completely for the cooling dynamics. Similarly, we find that at a higher carrier density of $n = 1.7 \times 10^{12} \text{ cm}^{-2}$, the hyperbolic cooling model has already begun to deviate from the experimental data for $T_L < 200 \text{ K}$ (Supplementary Fig. 10). Most probably, at sufficiently low lattice temperature and sufficiently high carrier density, cooling through optical phonons^{22,23} and momentum-conserving cooling to acoustic graphene phonons^{25,38,39} become the dominant channels.

In summary, we have addressed the issue of out-of-plane heat transfer in a device comprising hBN-encapsulated graphene. Combining experiments with microscopic theoretical calculations, we have shown that the dominant cooling channel is the one in which heat transfer from hot graphene carriers to the hBN polar substrate occurs via near-field coupling to hyperbolic phonon modes. This efficient mechanism explains the observation of a lower-than-expected cooling time in clean hBN-encapsulated graphene. We note that the observation of slower cooling for thin hBN encapsulation could have important implications for photo-detection applications. In addition, we predict that significantly slower cooling can be achieved using alternative layered dielectrics, such as MoS_2 . Furthermore, the near-field coupling we studied in this work between hot graphene carriers and hyperbolic hBN phonons may pave the way to novel approaches in fields such as nanophotonics, ultrahigh-resolution microscopy and nanoscale thermal management.

Methods

Methods, including statements of data availability and any associated accession codes and references, are available at <https://doi.org/10.1038/s41565-017-0008-8>.

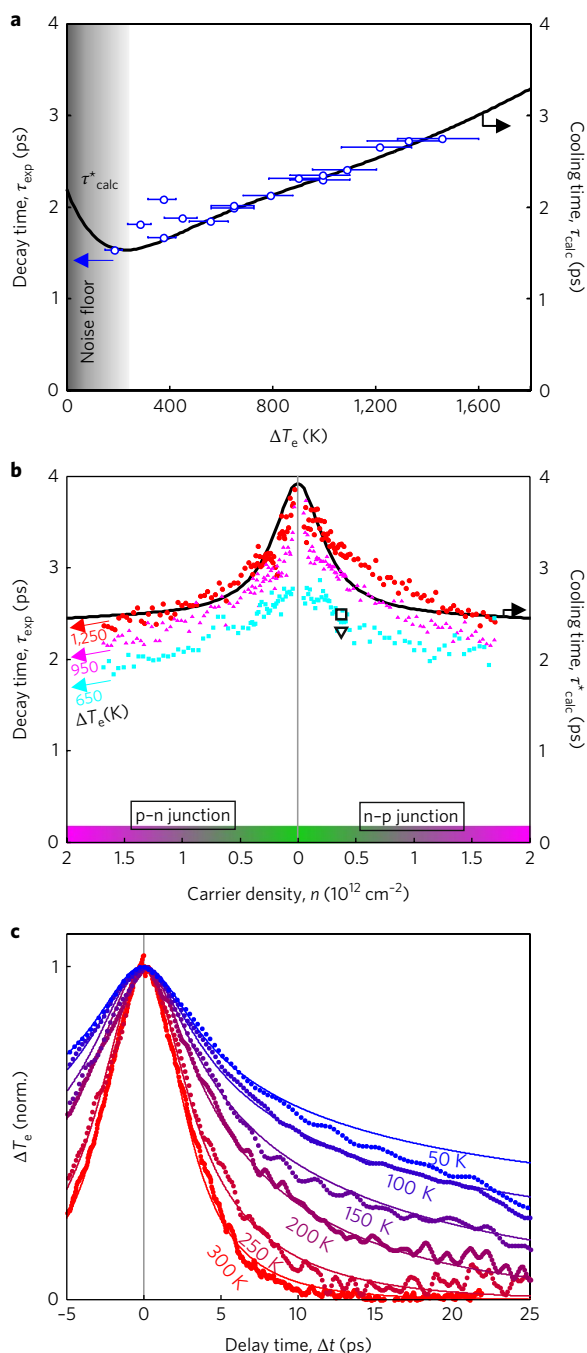


Fig. 4 | Quantitative comparison with hyperbolic hBN cooling. **a**, Comparison of measured decay time τ_{exp} (blue symbols and left axis) and calculated cooling time τ_{calc} (solid black line and right axis) as a function of electron temperature without any adjustable parameters. **b**, Measured decay time τ_{exp} (symbols and left axis) at room temperature as a function of carrier density for three different laser powers, compared with near-equilibrium cooling time τ_{calc}^* (solid line and right axis) according to super-Planckian cooling to hyperbolic hBN phonons without any adjustable parameters. The open square and triangle show the obtained decay time from time-resolved optical and terahertz spectroscopy, respectively, for $\Delta T_e = 600 \pm 200$ K. **c**, Comparison of the complete cooling dynamics as measured (data points) and calculated (solid line) for $n = 0.06 \times 10^{12} \text{ cm}^{-2}$ for varying lattice temperature. The calculated dynamics are convoluted with a Gaussian function representing the experimental time resolution. We find an initial temperature increase of $\Delta T = 300\text{--}500$ K for all temperatures, except 1,250 K for $T_l = 300$ K. The lower ΔT is related to the larger effective photocurrent spot size.

Received: 28 December 2016; Accepted: 20 September 2017; Published online: 27 November 2017

References

- Geim, A. K. & Grigorieva, I. V. Van der Waals heterostructures. *Nature* **499**, 419–425 (2013).
- Dean, C. R. et al. Boron nitride substrates for high-quality graphene electronics. *Nat. Nanotech.* **5**, 722–726 (2010).
- Mayorov, A. S. et al. Micrometer-scale ballistic transport in encapsulated graphene at room temperature. *Nano Lett.* **11**, 2396–2399 (2011).
- Britnell, L. et al. Electron tunneling through ultrathin boron nitride crystalline barriers. *Nano Lett.* **12**, 1707–1710 (2012).
- Dean, C. R. et al. Hofstadter's butterfly and the fractal quantum Hall effect in Moiré superlattices. *Nature* **497**, 598–602 (2013).
- Ferrari, A. C. et al. Science and technology roadmap for graphene, related two-dimensional crystals, and hybrid systems. *Nanoscale* **7**, 4598–4810 (2015).
- Wang, L. et al. One-dimensional electrical contact to a two-dimensional material. *Science* **342**, 614–617 (2013).
- Balandin, A. A. et al. Superior thermal conductivity of single-layer graphene. *Nano Lett.* **8**, 902–907 (2008).
- Britnell, L. et al. Strong light–matter interactions in heterostructures of atomically thin films. *Science* **340**, 1311–1314 (2013).
- Koppens, F. H. L. et al. Photodetectors based on graphene, other two-dimensional materials and hybrid systems. *Nat. Nanotech.* **9**, 780–793 (2014).
- Lopez-Sanchez, O. et al. Light generation and harvesting in a van der Waals heterostructure. *ACS Nano* **8**, 3042–3048 (2014).
- Bonaccorso, F. et al. Graphene, related two-dimensional crystals, and hybrid systems for energy conversion and storage. *Science* **347**, 1246501 (2015).
- Mics, Z. et al. Thermodynamic picture of ultrafast charge transport in graphene. *Nat. Commun.* **6**, 7655 (2015).
- Kim, Y. D. et al. Bright visible light emission from graphene. *Nat. Nanotech.* **10**, 676–681 (2015).
- Massicotte, M. et al. Picosecond photoresponse in van der Waals heterostructures. *Nat. Nanotech.* **11**, 42–46 (2016).
- Bonaccorso, F., Sun, Z., Hasan, T. & Ferrari, A. C. Graphene photonics and optoelectronics. *Nat. Photon.* **4**, 611–622 (2010).
- Caldwell, J. D. et al. Sub-diffractive volume-confined polaritons in the natural hyperbolic material hexagonal boron nitride. *Nat. Commun.* **5**, 5221 (2014).
- Dai, S. et al. Tunable phonon polaritons in atomically thin van der Waals crystals of boron nitride. *Science* **343**, 1125–1129 (2014).
- Basov, D. N., Fogler, M. M. & Garcia de Abajo, F. J. Polaritons in van der Waals materials. *Science* **354**, 1992 (2016).
- Gabor, N. M. et al. Hot carrier-assisted intrinsic photoresponse in graphene. *Science* **334**, 648–652 (2011).
- Song, J. C. W. et al. Hot carrier transport and photocurrent response in graphene. *Nano Lett.* **11**, 4688–4692 (2011).
- Kampftrath, T. et al. Strongly coupled optical phonons in the ultrafast dynamics of the electronic energy and current relaxation in graphite. *Phys. Rev. Lett.* **95**, 187403 (2005).
- Mihnev, M. T. et al. Microscopic origins of the terahertz carrier relaxation and cooling dynamics in graphene. *Nat. Commun.* **7**, 11617 (2016).
- Brida, D. et al. Ultrafast collinear scattering and carrier multiplication in graphene. *Nat. Commun.* **4**, 1987 (2013).
- Bistritzer, R. & MacDonald, A. H. Electronic cooling in graphene. *Phys. Rev. Lett.* **102**, 206410 (2009).
- Song, J. C. W., Reizer, M. Y. & Levitov, L. S. Disorder-assisted electron–phonon scattering and cooling pathways in graphene. *Phys. Rev. Lett.* **109**, 106602 (2012).
- Graham, M. W., Shi, S.-F., Ralph, D. C., Park, J. & McEuen, P. L. Photocurrent measurements of supercollision cooling in graphene. *Nat. Phys.* **9**, 103–108 (2013).
- Betz, A. C. et al. Supercollision cooling in undoped graphene. *Nat. Phys.* **9**, 109–112 (2013).
- Low, T. et al. Cooling of photoexcited carriers in graphene by internal and substrate phonons. *Phys. Rev. B* **86**, 045413 (2012).
- Hamm, J. M. et al. Nonequilibrium plasmon emission drives ultrafast carrier relaxation dynamics in photoexcited graphene. *Phys. Rev. B* **93**, 041408 (2016).
- Principi, A. et al. Super-Planckian electron cooling in a van der Waals stack. *Phys. Rev. Lett.* **118**, 126804 (2017).
- Banszerus, L. et al. Ultrahigh-mobility graphene devices from chemical vapor deposition on reusable copper. *Sci. Adv.* **1**, e1500222 (2015).
- Nyquist, H. Thermal agitation of electric charge in conductors. *Phys. Rev.* **32**, 110–113 (1928).
- Mihnev, M. T. et al. Electronic cooling via interlayer Coulomb coupling in multilayer epitaxial graphene. *Nat. Commun.* **6**, 8105 (2015).

35. Tomadin, A. et al. Accessing phonon polaritons in hyperbolic crystals by angle-resolved photoemission spectroscopy. *Phys. Rev. Lett.* **115**, 087401 (2015).
36. Giuliani, G. F. & Vignale, G. *Quantum Theory of the Electron Liquid*. (Cambridge Univ. Press, Cambridge, 2005).
37. Yang, W. et al. A graphene Zener–Klein transistor cooled by a hyperbolic substrate. *Nat. Nanotech.* <https://doi.org/10.1038/s41565-017-0007-9> 2017.
38. Ma, Q. et al. Competing channels for hot-electron cooling in graphene. *Phys. Rev. Lett.* **112**, 247401 (2014).
39. Jadidi, M. M. et al. Infrared nonlinear photomixing spectroscopy of graphene thermal relaxation. *Phys. Rev. Lett.* **117**, 257401 (2016).
40. Hwang, E. J., Rossi, E. & Das Sarma, S. Theory of thermopower in two-dimensional graphene. *Phys. Rev. B* **80**, 235415 (2009).
41. Wunsch, B. et al. Dynamical polarization of graphene at finite doping. *New J. Phys.* **8**, 318 (2006).
42. Hwang, E. H. & Das Sarma, S. Dielectric function, screening, and plasmons in two-dimensional graphene. *Phys. Rev. B* **75**, 205418 (2007).
43. Principi, A., Polini, M. & Vignale, G. Linear response of doped graphene sheets to vector potentials. *Phys. Rev. B* **80**, 075418 (2009).
44. Kotov, V. N. et al. Electron–electron interactions in graphene: current status and perspectives. *Rev. Mod. Phys.* **84**, 1067 (2012).
45. Alonso-González, P. et al. Acoustic terahertz graphene plasmons revealed by photocurrent nanoscopy. *Nat. Nanotech.* **2**, 31–35 (2017).

Acknowledgements

The authors thank A. Tomadin and F. Vialla for discussions. This work was supported by the European Union's Horizon 2020 research and innovation programme under grant agreement no. 696656, Graphene Flagship, Fondazione Istituto Italiano di Tecnologia, the Spanish Ministry of Economy and Competitiveness through the Severo Ochoa Programme for Centres of Excellence in R&D (SEV-2015-0522), Fundació Cellex Barcelona, Mineco grants Ramon y Cajal (RYC-2012-12281), Plan Nacional (FIS2013-47161-P) and the Government of Catalonia through an SGR grant (2014-SGR-1535), ERC StG CarbonLight (307806), ERC grant Hetero2D, and EPSRC

grants EP/K01711X/1, EP/K017144/1, EP/N010345/1 and EP/L016087/1. K.-J.T. acknowledges support from a Mineco Young Investigator Grant (FIS2014-59639-JIN). A.P. acknowledges support from ERC Advanced Grant 338957 FEMTO/NANO and from the NWO via the Spinoza Prize. M.M. acknowledges support from the Natural Sciences and Engineering Research Council of Canada (PGSD3-426325-2012). D.T. acknowledges financial support from the European Union Marie Curie Program (Career Integration grant no. 334324 LIGHTER) and the Max Planck Society. K.W. and T.T. acknowledge support from the Elemental Strategy Initiative conducted by the MEXT, Japan and JSPS KAKENHI (grant nos. JP26248061, JP15K21722 and JP25106006).

Author contributions

K.-J.T. and F.H.L.K. conceived the experiment. K.-J.T. and N.C.H.H. performed the time-resolved photocurrent experiments and performed data analysis. A.P., M.P. and M.B.L. developed the theory and performed calculations on hyperbolic cooling. E.A.A.P. performed the optical pump–probe spectroscopy measurements. Z.M. and K.-J.T. performed the optical pump–THz probe spectroscopy measurements. N.C.H.H., M.B.L., L.B., M.M., P.S., D.D., D.G.P., I.G., G.S. and A.L. fabricated devices. K.W. and T.T. contributed hBN material. M.B., D.T., C.S., A.C.F., G.C., M.P. and F.H.L.K. supervised the work and discussed the results. K.-J.T., F.H.L.K. and M.P. wrote the paper, with input from all authors.

Competing interests

The authors declare no competing financial interests.

Additional information

Supplementary information is available for this paper at <https://doi.org/10.1038/s41565-017-0008-8>.

Reprints and permissions information is available at www.nature.com/reprints.

Correspondence and requests for materials should be addressed to K.-J.T. or F.H.L.K.

Publisher's note: Springer Nature remains neutral with regard to jurisdictional claims in published maps and institutional affiliations.

Methods

Extraction of the initial hot carrier temperature. The measured photovoltage V_{PTE} scales with the time-averaged increase in electron temperature $\langle T_e - T_L \rangle$. In the case of cooling length smaller than the laser spot size (which is the case at room temperature) the relevant heat equation gives a simple linear scaling between peak and average increase in T_e , governed by the interfacial heat conductivity Γ . We assume that Γ and the Seebeck coefficient are constant with power⁴⁰, so that the photovoltage as a function of power directly represents the peak T_e increase as a function of power: $V_{\text{PTE}} = a(T_e - T_L)$. For undoped graphene, the peak T_e after illumination with laser power P is $T_e = \sqrt[3]{T_L^3 + bP}$, where b is a constant that depends on laser repetition rate f , absorption coefficient η_{abs} , heating efficiency η_{heat} and spot size L_{spot} . The cube root comes from the T^2 scaling of the electronic heat capacity for undoped graphene (we apply this analysis to a low carrier density of $0.06 \times 10^{12} \text{ cm}^{-2}$). By fitting V_{PTE} as a function of P , we extract the constants a and b , which allows us to recover the power-dependent peak T_e (Supplementary Fig. 7). We verify the obtained constant b and find good agreement when using

an absorption of $\eta_{\text{abs}} = 1\%$ (due to the layered dielectrics), a heating efficiency of $\eta_{\text{heat}} = 80\%$ and a spot size L_{spot} of $\sim 2 \mu\text{m}$.

Numerical calculations. Theoretical curves were obtained by numerically integrating equation (1)³¹. The non-local conductivity is connected to the density–density response function of graphene, $\chi_{mn}(k, \omega)$, by the formula $\sigma(\omega, k) = ie^2 \omega \chi_{mn}(k, \omega) / k^2$. Within the random-phase approximation, we approximate $\chi_{mn}(k, \omega)$ with its non-interacting expression, which is given in refs^{41–44}. Neglecting retardation effects, the surface admittance is connected to the screened Coulomb interaction between two electrons in graphene, $V(k, \omega)$, by the formula $Y(\omega, k) = -ie^2 \omega V^{-1}(k, \omega) / k^2$. The expression for $V(k, \omega)$ is given for graphene embedded into slabs of hBN and in the presence of non-hyperbolic dielectrics and metallic gates in ref.⁴⁵.

Data availability. The data that support the plots within this paper and other findings of this study are available from the corresponding author upon reasonable request.